Michael C. Haslam: Research Statement

Department of Mathematics and Statistics
York University, Ross S621
4700 Keele St., ON Canada M3J 1P3

Phone: (416) 736-2100 x44645
Email: mchaslam@mathstat.yorku.ca
URL: http://www.math.yorku.ca/∼mchaslam/

My professional research goals center around the investigation and solution of mathematical and computational problems of scientific and engineering relevance. During the last few years, I have worked on a variety of highly applied and very challenging problems in electromagnetics, hydrodynamics, and combinations of both; certainly, computational science lies at the core of my research interests.

The main goal of computational electromagnetics, for example, is the design and implementation of numerical methods that can be used to efficiently simulate electromagnetic wave interactions with complex material structures. This field has shown an impressive growth in recent years, as improved numerical algorithms enable accurate simulation of the ever more complex phenomena arising in an ever growing number of applications. The numerical methods used in this area draw from the classical approaches, such as the method of moments and finite-element based algorithms into the efficient high-order/accelerated algorithms that have arisen over the last two decades. Applications are found in communications (transmission through optical fiber or wireless communication), remote sensing and surveillance (radar and sonar systems), geophysical prospecting, materials science, and biomedical imaging (optical coherence tomography), to name but a few.

Significant challenges arise in the design of reliable numerical algorithms for engineering and industrial applications such as those mentioned above. These challenges are largely due to the necessity of numerical methods to resolve wave oscillations and interactions of these with geometrically and/or compositionally complex structures, which lead to very high (often prohibitive) computational costs for many problems of interest. Often times the approaches outlined below result in computation times which are several orders of magnitude smaller than those produced by the classic solution methods such as the method of moments. The focus of my work has been and will continue to be the development and implementation of efficient, fast and accurate numerical algorithms to enable treatment of challenging engineering and scientific applications.

1 Wire Antenna Problems

1.1 Straight Wires

The problem of evaluating the current distribution that is induced on a thin straight-wire antenna by a time-harmonic electromagnetic field was first described by Pocklington [1] more than a century ago; its computation remains an important and difficult engineering problem to this day. The current J induced on a wire occupying the interval $[-1, 1]$ by an incident electric field with axial component e and wave number k can be obtained as a solution of the Pocklington integro-differential equation

$$\left(\frac{\partial^2}{\partial z^2} + k^2\right) \int_{-1}^{1} G(z-t)\, J(t)\, dt = -4\pi i k e(z), \tag{1}$$

subject to the end-point conditions $J(-1) = J(1) = 0$. An alternative (and, in exact arithmetic, equivalent) formulation for this problem is given by the Hallén integral equation, which results from (1) by inverting the Helmholtz operator.

The solution of both the Pocklington and Hallén problems has received wide attention, owing to the importance and age of the problem. We believe that we have made significant contributions to the literature in [2]. One of the main results in that paper is a regularity proof which, in the particular case of a time-harmonic incident plane wave implies that, for a straight wire occupying the interval $[-1,1]$, the current is given by $J(z) = I(z)/\sqrt{1-z^2}$ where $I(z)$ is an *infinitely differentiable* function. (The strongest previous result in these regards has I as a twice continuously differentiable function at most.) The second focus of this work is numerics: we present three *super-algebraically convergent* algorithms for the solution of wire problems, two of which are based on Hallén's integral equation, while the third one is based on the Pocklington integro-differential equation. The kernel $G(z)$ that appears in these formulations, which is itself given by an integral, has a logarithmic singularity at $z = 0$. Both our regularity proof and our strategy to produce algorithms of high order of accuracy for this problem are based on two main elements. On one hand we 1) Introduce a new decomposition of the kernel of the form $G(z) = F_1(z)\ln|z| + F_2(z)$, where $F_1(z)$ and $F_2(z)$ are analytic functions in the domain $|z| < \infty$. On the other hand, we 2) Account to high order for the end-point square root singularities in the current.

Having accounted to all orders for all integrand singularities and near-singularities, and in view of our regularity result, we find that the Hallén- and Pocklington-based algorithms we propose converge super-algebraically: faster than $\mathcal{O}(N^{-m})$ and $\mathcal{O}(M^{-m})$ for any positive integer m, where N and M are the numbers of unknowns and and the number of integration points required for construction of the discretized operator, respectively. (Interestingly, in contrast with reports and comments concerning previous methods, we found that our Hallén-based and Pocklington-based algorithms are equally efficient in many cases, and that there are important instances in which the Hallén-based methods are preferable while, in others the Pocklington-based approach is more favorable.) In previous studies, at most the leading order contribution to the logarithmic singular term was extracted from the kernel and treated analytically, the higher-order singular derivatives were left untreated, and the resulting integration methods for the kernel exhibit $\mathcal{O}(M^{-3})$ convergence at best. In many cases, to achieve a given accuracy, the numbers N of unknowns required by our codes are up to a factor of four times smaller than those required by the best solvers available previously [3]; the required number M of integration points, in turn, can be several orders of magnitude smaller than those required in previous methods.

Subsequent to our development of wire-scattering solver mentioned above we pursued a project, in collaboration with O. Bruno and R. Paffenroth (Caltech) and V. Cable and N. Bleyzunk (JPL), to interface this solver with Caltech's fast and accurate integral equation solvers for general electromagnetic problems, including scattering from surfaces containing edges and corners. The goal of this collaboration was to create a fully validated EM simulation infrastructure for use by the Spacecraft Antennas Research Group of the NASA Jet Propulsion Laboratory (JPL). The combined wire and edge solvers have been used to produce the far-field of a experimental configuration consisting of cylinder with an attached cylindrical monopole antenna, showing excellent agreement with experimental data obtained by our JPL collaborators. These and other results are presented in [4]. The tools resulting from this effort will be used to plan, design and optimize UHF proximity links between orbiters and surface landers, and between different surface assets for all Mars missions.

1.2 High-Order Treatment of Driving Sources

A related, but more difficult problem consists of the case when the excitation source (such as a coaxial line) is attached to the wire itself, giving rise to the so-called transmit problem. The most common current source model is the so-called delta-gap generator, in which a finite voltage driving the current is maintained across an infinitesimally thin gap at the source location. Prior to our work, the precise nature of the singularity in the current distribution induced by a source was known only at leading order, and hence the error of related numerical methods were limited to second order in the number of discretization (mesh) points. High-order methods rely on precise knowledge of all singular terms in a local series expansion of the current about the source. We have shown that the singularity in the current distribution due to the source may be deduced to all orders by means of an expansion based on a related, but simpler integral equation. The resulting numerical implementations have demonstrated high-order convergence [5].

To generate high-order algorithms for the driven-wire case we extend the scattering-problem algorithm described in [2]. If the wire is taken to lie on the interval $z \in [-1, 1]$ with the delta gap located at $z = 0$, for example, then the current density $J = J(z)$ can be found as the solution of the Hallén equation

$$\int_{-1}^{1} G(z-t)\, J(t)\, dt = \frac{2\pi i V}{\zeta_0} \left(\sin k|z| + \alpha \cos kz\right), \tag{2}$$

subject to the end-point conditions $J(-1) = J(1) = 0$. Here $\zeta_0 = 120\pi\ \Omega$ is the free-space impedance, k is the free-space wave number, and α is a constant chosen to ensure the vanishing of the current at the wire end points. It is known that the solution to the Hallén equation (2) in this case possesses a logarithmic singularity at leading order [6], which gives rise to low order convergence and, indeed, large numerical errors in all the methods we have found in the literature. Notably, for example, in the recent work on driven wires [7] we read:

> "Note that the interpretation of convergence for wire antennas excited with a delta-gap voltage source should be based on the current distribution excluding the current near the source, where the imaginary part of the current at the delta-gap source eventually diverges as the sub-domain size decreases... A convergence study was done by illuminating a wire loop with a normally incident plane wave at 1 GHz. Using a plane wave excitation eliminates the slow convergence associated with the infinite feed capacitance of a delta-gap source."

In order to address the important problem of the regularity of the current density in the transmit case and to produce fast, high-order convergence in spite of this difficulty our ongoing work has obtained the following form for the solution of the Hallén equation:

$$J(z) = \frac{2\pi i V}{\zeta_0} \left[I_0(z) \ln\left(\frac{1+\sqrt{1-z^2}}{1-\sqrt{1-z^2}} \right) + \frac{I_1(z)}{\sqrt{1-z^2}} \right], \tag{3}$$

where I_0 is an explicitly computable function and I_1 is a *smooth* function to be evaluated numerically. This approach thus effectively regularizes the singularity problem and paves the way for high-order solution of the driven antenna problem. In detail, using the power series expansion

$$I_0(z) = -\frac{ka}{\pi} \sum_{n=0}^{M} \alpha_{2n} \left(\frac{z}{2a}\right)^{2n}, \tag{4}$$

our method produces the coefficients α_{2n} as the solution of the linear system

$$\sum_{m=0}^{n} b_{2n-2m} \alpha_{2m} \sum_{\ell=0}^{n-m} \binom{2n-2m}{2\ell} \frac{1}{2\ell+2m+1} = \frac{(-1)^{n+1}(2ka)^{2n+1}}{2\pi k a^2 (2n+1)!} \tag{5}$$

for $n = 0, 1, \ldots, M$. Note that b_{2n} are the Taylor series coefficients of the kernel function F_1 (see section 1.1); an expression for b_{2n} is easily derived from expressions given in [2]. With the coefficients so chosen, the integral operator acting on the logarithmic term in (3) precisely cancels increasing powers of $k|z|$ arising from a Taylor series expansion of $\sin k|z|$ in the source function of equation (2). This method allows for the extraction of arbitrarily many orders of singularity from the source function h. Theoretical results in [2] imply then the function I_1 becomes increasingly smooth in the neighborhood of the driving point, and thus a Chebyshev discretization for this function becomes increasingly rapidly convergent. For reference the first few coefficients of I_0 in equation (4) are

$$\alpha_0 = 1, \quad \alpha_2 = 1 + 2(ka)^2, \quad \alpha_4 = -\frac{19}{12} + 2(ka)^2 + 2(ka)^4. \tag{6}$$

Our methods as outlined above fully resolve the current function I_1 everywhere on the interval $z \in [-1, 1]$, and in particular in a neighborhood of the origin.

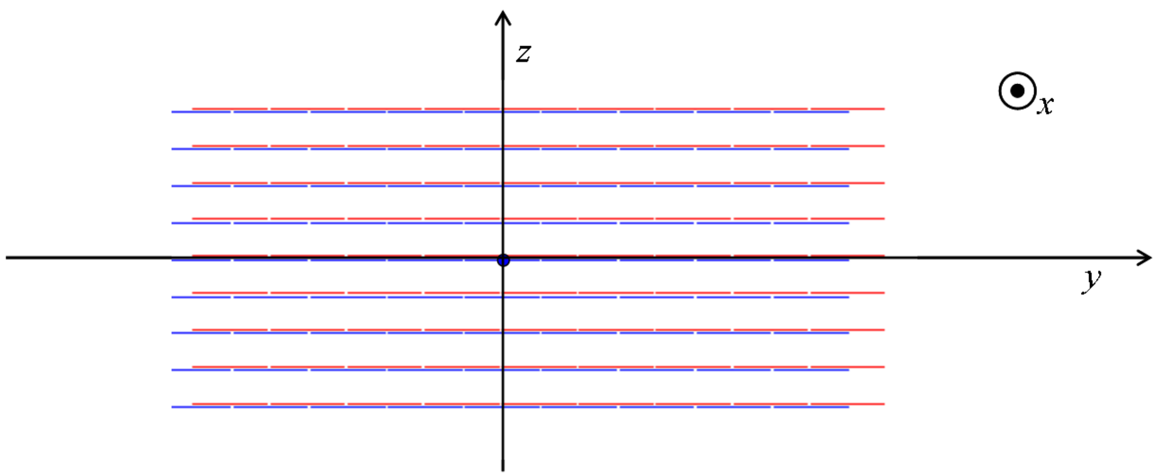

Figure 1: The 162-element array consists of two shifted coplanar 9x9 arrays. Each wire is 61mm in length and of diameter 0.0078mm. The red array is shifter from the blue array by 1.53mm in the vertical direction and 30.5mm to the right. The blue dot shows the position of the voltage driving source, located at the center of the central blue wire. Note that the array is not precisely symmetric with respect to the origin.

1.3 Large Driven Arrays of Wires

We have combined the computationally efficient approaches for the treatment of straight wires and on-wire sources to produce very fast solvers for driven arrays consisting of *arbitrarily* large numbers of elements [8]. Such an extension of our methods has posed serious challenges: the possibility exists for two conducting elements to be in very close proximity to one another, and thus strongly interact, and potentially requiring significant refinement of computational grids. In what follows we outline our numerical results for such a large wire array where elements are placed in close proximity to one another.

The array geometry is depicted in Figure 1. The array is driven by a current source located near the geometric center (and indicated as a blue dot at the origin on the figure). A selection of far-field results corresponding to an excitation frequency of 2GHz are depicted in Figure 2.

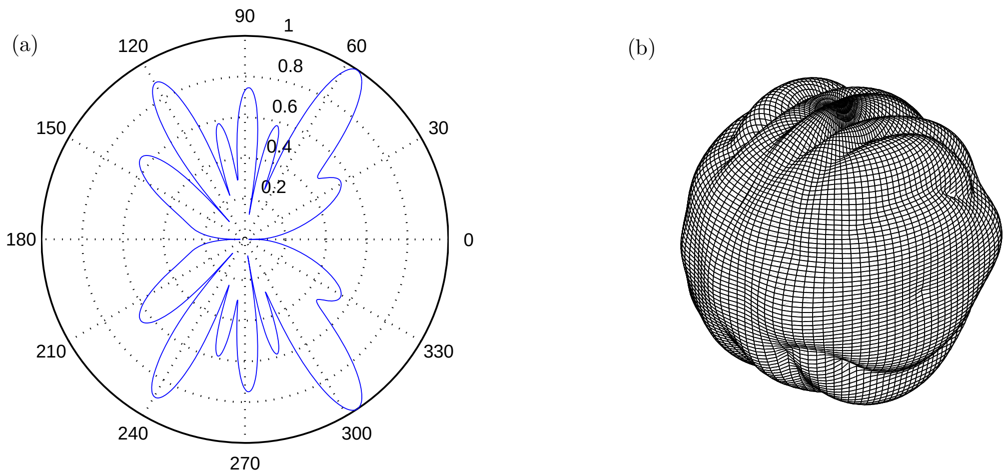

Figure 2: Far field analysis for 162-element antenna excited at 2GHz. (a) Total (normalized) far field intensity in the yz-plane; (b) Three dimensional spherical plot of total field intensity at 2GHz.

1.4 Long Curved Wires and Backscattering Problems

Another important contribution we have made to the study of thin wire antennas is a numerical method to treat the scattering problem from fully three-dimensional long curvilinear wires (in contrast to the straight wire case discussed above). In that work [9] we have presented a method which fully resolves the singularity of the three-dimensional integral equations, including effects generated by the local curvature of the antenna. Previous methods utilized a tangent plane approximation, locally replacing the curved wire by a straight wire in the neighborhood of the kernels singularity, and thus were limited to second order in the mesh discretization. Our numerical implementations for long curvilinear antennas have demonstrated exponential convergence in the number of mesh points.

For curved wires we utilize the full Pocklington-type equation, and associated kernel, since the Hallén type equation for the curved-wire case is unduly complex; the Pocklington equation for a wire parameterized by $s \in [-1, 1]$ with tangent vector $\hat{\mathbf{t}}(s)$ reads

$$\frac{\partial}{\partial s} \int_{-1}^{1} \frac{\partial}{\partial s'} J(s') G(s, s')\, ds' + k^2 \int_{-1}^{1} \hat{\mathbf{t}}(s) \cdot \hat{\mathbf{t}}(s') J(s') G(s, s')\, ds' = e(s), \tag{7}$$

where the source term $e(s)$ is proportional to the tangential incident field. The curved-wire kernel is not translation-invariant, and, thus, for fast performance, it is imperative to obtain a highly efficient method for evaluation of this quantity. We have noted that the curved wire kernel may be written in a similar for to the straight-wire kernel in [2]:

$$G(s, s') = \frac{1}{2\pi\sqrt{aw}} \int_0^{\pi} \frac{\mathrm{e}^{2ik\sqrt{aw}\sqrt{\rho^2+\sin^2\psi}}}{\sqrt{\rho^2 + \sin^2\psi}}\, d\psi. \tag{8}$$

The kernel (8) which depends on non-dimensional quantities $w = w(s, s')$ and $\rho = \rho(s, s')$, can be obtained extremely rapidly by means of the series expansion

$$G(s, s') = \frac{ik}{\sqrt{\pi}} \sum_{m=0}^{\infty} \frac{(k^2 aw)^{2m} \Gamma(m + 1/2)}{m!(2m)!} \frac{h_{2m}^{(1)}(kv)}{(kv)^{2m}} \tag{9}$$

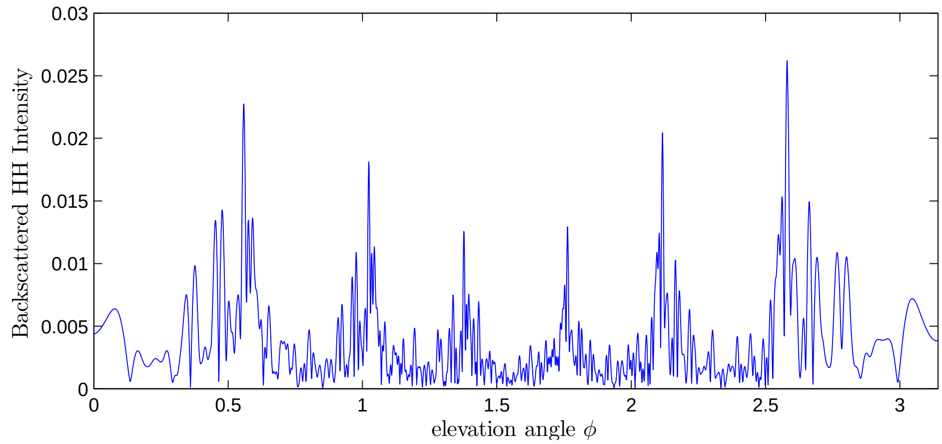

Figure 3: Backscattered HH intensity for long helix lying on the x-axis. Wire parameters are $t = 50$ turns, $\ell = 60.96$cm and $r = 6.35$cm; the diameter of the wire is 0.255mm. Interesting resonances are present at regular intervals in the elevation angle.

(where $v = v(w, \rho)$) for s sufficiently far from s'.

The high-order curved wire algorithm we have produced generates solutions of an accuracy similar to that provided by the straight wire solver, in comparable, very fast computing times. As an interesting example we consider a left-handed helical wire lying on the x-axis: the Cartesian components of the helical filament are given by $x = ps$, $y = r\cos[t\pi(s+1)]$, $z = -r\sin[t\pi(s+1)]$, where p is the pitch, t is the number of turns, and r is the loop radius. We may further relate the pitch p to the turn spacing ℓ: $p = t\ell/2$. The helical wire is illuminated by a polarized incident plane wave with direction vector $\mathbf{r} = (\cos\theta\cos\phi, \sin\theta\cos\phi, -\sin\phi)$. The currents excited by the incident field are computed and far field results, which are often the desired result in applications, are produced. In Figure 3 we show the backscattered electric field intensity in horizontal polarization produced by a horizontally polarized incident field (the well-known HH case) with azimuthal angle $\theta = 0$. We note the interesting resonances which appear in the backscattered direction as the elevation angle ϕ varies from 0 to π.

2 Numerical Methods for Optical Gratings

The phenomenon of scattering of waves by periodic surfaces is of fundamental importance in optics and numerous other applications in the physical sciences. For example, diffraction gratings are used in solar energy research, remote sensing applications, and quality control processes in the microelectronics industry. A vast literature exists for scattering from periodic surfaces, encompassing a wide variety of methods. In what follows we present methods based on the theory of integral equations.

Our high-order algorithms for grating diffraction problems treat the scattering of a time-harmonic incident plane wave of wavelength $\lambda = 2\pi/k$,

$$u_{inc}(\mathbf{r}) = \exp[i\,(\alpha x - \beta z)] \quad \text{with} \quad \alpha = k\cos\theta \quad \text{and} \quad \beta = k\sin\theta, \tag{10}$$

by a piecewise smooth P-periodic parametric perfectly conducting surface $\partial\mathcal{S}$. The total field $u(\mathbf{r})$, which equals the sum $u(\mathbf{r}) = u_{inc}(\mathbf{r}) + u_s(\mathbf{r})$ of the incident field u_{inc} and the (radiating) scattered field u_s, satisfies the scalar Helmholtz equation

$$\Delta u + k^2 u = 0 \quad \text{for} \quad \mathbf{r} \in \mathcal{S}, \tag{11}$$

a/P	N	M	N^*	error (TE)	$\|1-E\|$ (TE)	error (TM)	$\|1-E\|$ (TM)	t_{exe} (min)
4	550	2^{11}	700	7.35×10^{-13}	5.73×10^{-12}	7.58×10^{-13}	1.09×10^{-12}	10
8	1050	2^{12}	1200	6.14×10^{-12}	1.48×10^{-11}	7.52×10^{-11}	5.19×10^{-11}	64
12	1600	2^{13}	1700	1.49×10^{-11}	4.00×10^{-12}	3.75×10^{-11}	8.28×10^{-11}	236
16	2100	2^{13}	2200	3.59×10^{-11}	8.72×10^{-11}	5.74×10^{-11}	2.83×10^{-11}	392
20	2600	2^{13}	2700	9.80×10^{-11}	3.51×10^{-11}	2.05×10^{-10}	1.55×10^{-10}	570

Table 1: Code performance for various surface heights a with parameters and resulting accuracy and energy balance for both cases of TE and TM scattering from surface profile $f(x) = a\cos(2\pi x/P)$ with $\lambda = 0.05P$ and $\theta = 7\pi/18$.

where $\mathcal{S}$ is the region of the (x, z)-plane which lies above $\partial\mathcal{S}$. The TE and TM boundary-value problems for the Helmholtz equation result as the respective boundary conditions

$$u = 0 \quad \text{(TE)} \quad \text{and} \quad \frac{\partial u}{\partial \mathbf{n}} = 0 \quad \text{(TM)} \tag{12}$$

are imposed on the boundary $\partial\mathcal{S}$. The solutions of equation (11) for both TE and TM polarizations can be expressed in terms of double-layer potentials of the form

$$u_s(\mathbf{r}) = \int_{\partial\mathcal{S}} \frac{\partial\Phi(\mathbf{r},\mathbf{r}')}{\partial\mathbf{n}(\mathbf{r}')}\,\mu(\mathbf{r}')ds(\mathbf{r}'), \qquad \mathbf{r} \in \mathcal{S}, \tag{13}$$

where μ is an (unknown) surface density function and where $\Phi(\mathbf{r},\mathbf{r}') = iH_0^{(1)}(ik|\mathbf{r}-\mathbf{r}'|)/4$ is the two-dimensional radiating free-space Green's function [13]. The surface densities μ^+ and μ^- associated with TE and TM polarizations are solutions of the integral equations

$$-u_{inc}(\mathbf{r}) = \pm\frac{1}{2}\,\mu^{\pm}(\mathbf{r}) + \int_{\partial\mathcal{S}} \frac{\partial\Phi(\mathbf{r},\mathbf{r}')}{\partial\mathbf{n}(\mathbf{r}')}\,\mu^{\pm}(\mathbf{r}')\,ds(\mathbf{r}'), \qquad \mathbf{r} \in \partial\mathcal{S}, \tag{14}$$

where the $+$ and $-$ signs correspond to the TE and TM polarization cases, respectively.

2.1 Fast and Accurate Solution for Classical Gratings

In our contribution [10] we present an algorithm for evaluation of the integral equation (14) for scattering by one-dimensional, perfectly conducting smooth periodic surfaces $z = f(x)$ for both TE and TM polarizations. Our high-order algorithm for these problems is based on concurrent use of Floquet and Chebyshev expansions. For an incident field with C^∞ smoothness, our algorithms converge faster than $\mathcal{O}(N^{-m})$ and $\mathcal{O}(M^{-m})$ for all positive integers m, where N denotes the number of surface-density unknowns, and M denotes the number of weights used for integration of the kernel functions. For grating-diffraction problems in the resonance regime (heights and periods up to a few wavelengths) the proposed algorithm produces solutions with full double precision accuracy in computing times of the order of a few seconds—on present-day single processor PC-type desktops. The algorithm can also produce, in reasonable computing times, highly accurate solutions for very challenging grating diffraction problems, such as a) A problem of diffraction by a grating for which the peak-to-trough distance equals forty times its period which, in turn, equals twenty times the wavelength; and b) A high-frequency problem with very small incidence, up to and including 0.01 degrees from glancing. The qualities of the algorithm derive, in part, from use of certain integration weights that are computed accurately by means of an asymptotic expansion as the number of integration points tends to

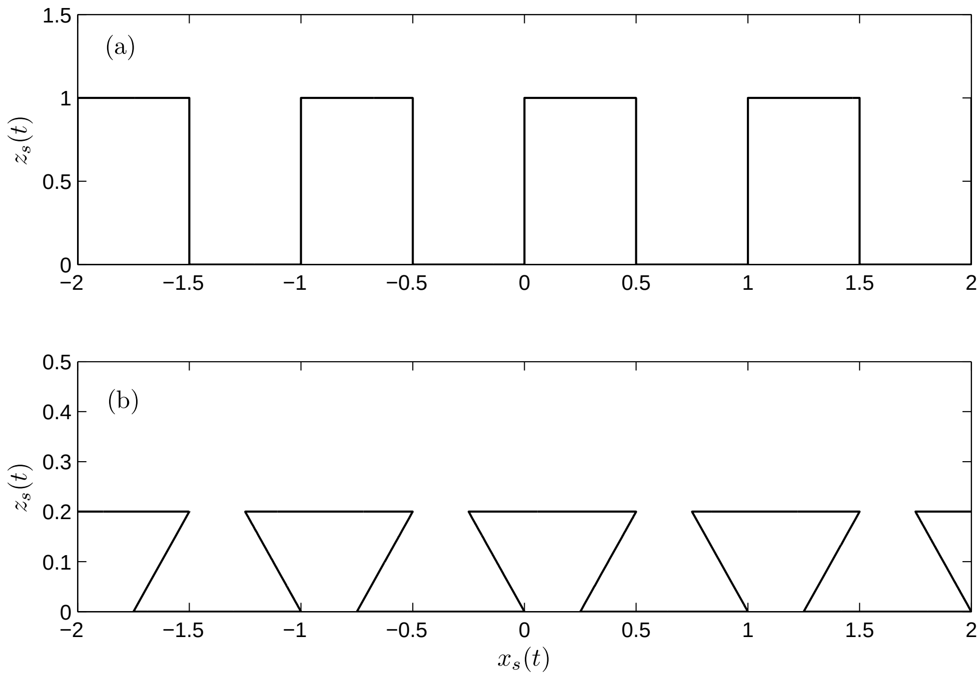

Figure 4: Several periods of the singular grating profiles $\mathbf{s}(t)$: the lamellar grating with $P = A = 1$ in (a); a test surface containing partial cavities with $P = 1$ and $A = 1/5$ in (b).

infinity. The algorithms presented in [10] are fully rigorous and convergent and, in particular, they take into account all scattering effects including shadowing and multiple reflections.

To demonstrate the robustness of that solver, we consider several cases that, to the best of our knowledge, could not previously be successfully tackled on desktop PCs. In Table 1 we consider problems with incidence angle fixed at a moderate value and with a moderate value of the frequency (supporting 40 propagating modes); the amplitude of the profile, in turn, is allowed to vary between 4 and 20 (i.e. the peak-to-trough height varies between 8 and 40 times the period). In each case near machine precision accuracies are produced in both the absolute error, and the classical energy balance estimate $|1 - E|$. The case $a/P = 4$ was previously considered in [15]; the most accurate method presented in that reference requires times of the order of 662 min. on a Sparc 20 workstation to achieve 4-digit accuracies for this problem. Our method, in contrast, achieves nearly double precision accuracies in computing times on the order of 10 min in this case.

2.2 Singular Vector-Parametric Gratings

In a companion work to [10] outlined above, we extend the methodology to *vector-parametric, possibly non-smooth* periodic scattering surfaces defined by a piecewise smooth vector parametrization of the form $\mathbf{s}(t) = (x_s(t), z_s(t))$. Like its single-valued smooth-surface counterpart, the solver is based on use of Floquet expansions and Chebyshev-based integration: the novel introduction of rapidly convergent Floquet expansions for currents on (possibly) non-smooth, multiple-valued scattering surfaces enables extension of the previous high-order methodology to a significantly broader class of important diffraction problems. In particular, our new method yields near machine precision accuracies in computing times of the order of a few seconds for scattering problems in the resonance regime,

N	M	With Regularization			Without Regularization		
		error	$\|1-E\|$	t_{exe}(s)	error	$\|1-E\|$	t_{exe}(s)
150	2^{10}	2.15×10^{-3}	1.01×10^{-3}	104.2	2.80×10^{-3}	9.39×10^{-3}	103.7
175	2^{10}	5.31×10^{-6}	7.01×10^{-6}	124.6	4.11×10^{-4}	1.54×10^{-4}	123.9
200	2^{10}	6.63×10^{-9}	2.23×10^{-9}	146.1	5.46×10^{-6}	5.75×10^{-6}	145.6
225	2^{10}	1.59×10^{-9}	6.44×10^{-11}	167.6	4.22×10^{-6}	8.90×10^{-6}	167.1
250	2^{10}	4.19×10^{-11}	1.74×10^{-11}	189.5	6.98×10^{-7}	7.94×10^{-7}	188.9

Table 2: Convergence results for singular grating profile in Figure 4(b) with $A/P = 1/5$. Together with integration points M, the error, energy balance and execution time are shown for the case of TE polarization with $\lambda = 0.05P$ (40 propagating modes) and $\theta = \pi/4$. Sets of results are presented for this problem when regularization is applied and otherwise. Clearly regularization gives rise to significantly faster and more stable convergence with a negligible cost.

and it can also produce, in reasonable computing times, solutions for highly challenging TE and TM scattering problems—defined by very deep multi-valued scattering surfaces and high frequencies of radiation—including cases in which non-smooth bounding surfaces enclose open cavities.

In the presence of geometric singularities in the surface profile, we actually solve a modified form of the integral equation (14). Indeed, in this case the integrands cannot be bounded by a function of the form $T(t-\tau)$, where $T = T(r)$ is an integrable function which is itself bounded for values of r away from $r = 0$. If left untreated, such singularities give rise to certain reductions in accuracy, as demonstrated below. Such a "bounded-integrability" property and an associated increased degree of accuracy can be restored through treatment of the leading order singularity in the integral equation's kernel at corner points. In order to restore bounded-integrability in the case in which the domain contains corners we note that the leading order singularity of the kernel of equation (14) coincides with the leading order singularity in the $k = 0$ (Laplace) Green's function. Indeed a vanishing term is formed by integrating the Laplace Green's function with the surface density at the source point. Subtracting out of the null terms from the original integral equation (14) results in a bounded-integrable integrand, and hence suitable for high-order numerical approximation by means of graded meshes such as those presented in [13] and references therein.

In order to demonstrate the advantages arising from use of the regularization discussed above, we compare the performance of our solver when applied to the regularized and non-regularized integral equations. To add substance to the example the comparison is made for a rather challenging problem, involving the singular parametric "open cavity" profile depicted in Figure 4(b) —and the wavelength $\lambda = 0.05P$ (giving rise to 40 propagating modes). In Table 2 convergence results are shown for the case of TE polarization; similar results are obtained in the TM case. The results presented in Table 2 show that inclusion of the regularization term requires a negligible amount of additional computational time over that needed in the non-regularized implementation, has a significant effect in the solution accuracies.

We have also used our singular profile solvers to demonstrate interesting physical behavior in an otherwise well-known grating geometry – the lamellar diffraction grating depicted in Figure 4(a) [12]. The well-known Wood-Rayleigh anomalies which may strongly influence scattering, particularly in the case of TM (vertical) polarization, occur at fixed wavelengths determined by the period of the surface and the direction and wavelength of the incident radiation. We demonstrate the presence of other anomalies which do not occur at the Wood-Rayleigh wavelengths and may play a dominant role in the scattering process. We show that the wavelengths at which these poorly-understood anomalies occur are determined by the geometrical features of the surface.

2.3 Three Dimensional Gratings and Layered Dielectric Gratings

I currently have a graduate student in Astronomy and Physics at York University working on efficient methods for acoustic scattering from three-dimensional plane periodic surfaces (funded by the Natural Sciences and Engineering Research Council of Canada). This is related to a project with with P.C. Gibson (York) and M. Lamoureux (Calgary) on the Pseudo-differential Operator Theory and Seismic Imaging (POTSI) project.

I have a working extension of the two dimensional codes discussed in this section applicable to layered dielectric media [14].

3 Enhanced Radar Backscatter From the Ocean Surface

Field and laboratory measurements of electromagnetic scattering from water waves are usually taken with a radar system in which there are separate facilities (antennas) to transmit and receive electromagnetic signals. While the transmitted energy is scattered in a number of directions by the water surface, the radar only receives the signals which are scattered in the direction in which the signal originated. Thus, studies of scattering from the ocean surface amount to analyzing the so-called *backscattered* signals, and deducing local surface features from these signals.

At low grazing angles (LGA), high frequency radar returns from the ocean surface exhibit qualitative features which stand in striking contrast to the returns corresponding to high grazing angle backscatter. Radar observations in the LGA regime indicate that the backscattered intensity in a resolution cell can increase dramatically in a time of the order of 0.1 seconds. While this behavior may be seen in both HH (horizontal transmitted, horizontal received) and VV (vertical transmitted, vertical received) polarizations, observations indicate that it is more intermittent and impulsive in HH. These sea-spikes, as they are colloquially known, are typically characterized by a ratio of the HH to VV polarization amplitude return which exceeds unity. A detailed understanding of this phenomenon has important consequences in the context of detection algorithms for surface targets; a sea spike is often associated with a false positive identification. Improved (remote) measurements of local wind conditions and sea states could also result.

While it had long been assumed that sea-spike events were strictly related to breaking waves, the field experiments of Lewis and Olin [20] were some of the first to suggest otherwise. From various shore sites, they measured X-band (6 - 12 GHz) radar returns from breaking and near-breaking waves, with simultaneous video recording of the visual features of the illuminated portions of the surface. Indeed, their data confirmed that very high amplitude sea spikes are associated with the development and decay of the whitecaps on waves. However, their data also clearly showed similarly structured backscatter in the absence of breaking waves, with video recordings indicating locally smooth surface profiles. A number of experimental studies followed with emphasis on the development of steep waves, early in the breaking process, and its effect on radar backscatter.

The primary aim of my doctoral thesis was to investigate the physical processes related to the stability of steep gravity waves, and their effect on the the scattering of electromagnetic waves. It has been known for some time that periodic water waves are subject to a variety of shape-altering instabilities. It is generally believed that a class of these instabilities, which are relevant to steep waves, are responsible for spilling breakers (See Section 4 below). Empirical and theoretical research on these instabilities has suggested that the dominant mechanism in nonlinear interactions in the wave field results in three-dimensional periodic structures.

An extended boundary condition method, commonly used in optical studies, is formulated to compute the scattering from of an electromagnetic plane wave of arbitrary polarization incident upon an arbitrary doubly periodic surface. This particular generalization of the method, which we provide for the first time, allows for the exact calculation of the fields corresponding to a linear, isotropic conducting dielectric scatterer. Results from commonly-used test cases were shown to compare very favorably with those from other methods presented in the literature. The full water wave equations are solved numerically, and highly accurate solutions corresponding to three-dimensional steep wave instabilities are obtained. The scattered electromagnetic fields resulting from these profiles are then computed using the extended boundary condition method. The computational requirements of the method are large, necessitating the parallel implementation of routines on a Sharcnet-Canada 144 processor computing cluster. Results for a number of incidence angles are examined for surface wave configurations in the process of undergoing these instabilities. It is found that, under some circumstances, returns may drop several orders of magnitude as a result of small variations in the angle on incident radiation. Furthermore, it is shown that these anomalous returns are not the result of the well-known Rayleigh anomaly, which corresponds to the passing off of a spectral order. Returns with HH to VV polarization ratios greater than unity, which are characteristic of sea-spike events, have been observed.

Work toward my doctoral degree was carried out both at the University of Western Ontario, and in the Aerospace Radar and Navigation Section of Defence Research Establishment Ottawa (DREO), where I was a visiting student in the academic year 1999-2000. A proper understanding of the dynamical aspects of sea-spikes is of great interest in coastal surveillance applications. The scattering algorithms used in my Ph.D. studies should show significant improvements in efficiency when redesigned in the spirit of the fast high-order solvers I have been pursuing recently—a project we intend to pursue in the near future. While such an approach would still require large computing resources,I believe a detailed understanding of enhanced radar backscatter will emerge from this effort. High resolution empirical data collected by DREO, to which we have been given access, will be used to confirm our numerical studies.

4 Hydrodynamic Stability Problems

4.1 Stability of deep-water gravity waves

Observations of water waves in nature indicate that they usually do not propagate as a single monochromatic or quasi-monochromatic wave train. Instead, especially on the open ocean or when shoaling on beaches, they may assume much less regular patterns. In general, the motion of water waves is subject to a variety of physical processes, including the intrinsic instabilities in their motion, surface tension effects, and dissipative processes such as shearing by a wind input, or wave breaking. All of the aforementioned processes may contribute to some degree or another to determine the overall wave profile and its time evolution.

Wave breaking is a complicated nonlinear phenomenon which exhibits a wide range of physical behavior. Wave breaking represents one of the most long-standing problems of water wave theory; the dynamics of these processes remain poorly understood. As a propagating wave begins to reach its maximum energy state, breaking first appears as foam and bubbles on the crests of the steepest waves. In this stage, known as a *spilling breaker*, the crest is symmetrical, or nearly so, and the process is usually accompanied by a small amount of dissipation. This stage of wave breaking is of great interest in the study of radar signal enhancements (see Section 3.) It is known that steep waves are subject to rapidly growing instabilities, which in turn lead to breaking. McLean [21] has shown that the so-called Class-II instabilities, which are dominant for steep waves, result in three-

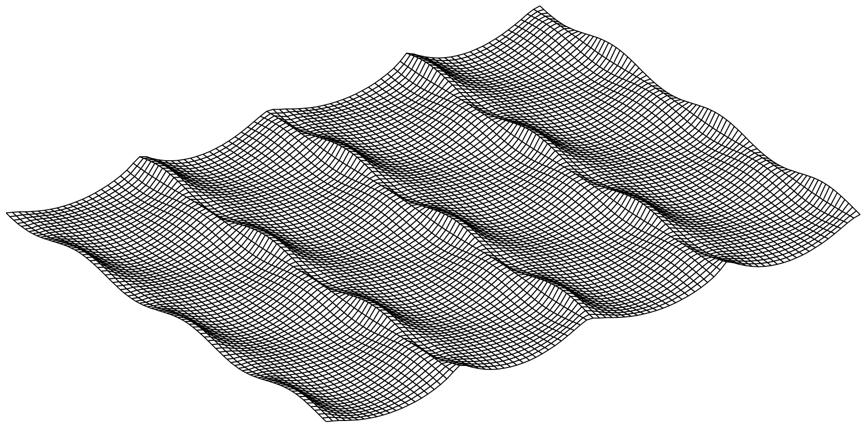

Figure 5: Stokes wave train with height-to-wavelength ratio 0.127 undergoing Class II instability. Local surface features which develop on the crests of the waves are thought to lead to spilling breakers.

dimensional crescent-shaped patterns co-propagating with the unperturbed wave. It appears that the crescent-shaped Class-II instability may locally increase the wave slope at the crest of steep waves beyond the maximum value, resulting in the spilling breakers. To fully understand the effects of these instabilities on the scattering of electromagnetic waves, we have implemented a variation of the numerical approach of McLean [21]. We obtain highly accurate solutions for both, the base Stokes wave, and the evolution of the superimposed disturbance (See Figure 5, for example).

4.2 Modal interactions in a Bickley jet

For the plane wakes and jets considered in our studies, it is well-known that there may be two different types of neutral modes with critical layers centered on the inflection points, viz. the sinuous and varicose modes. The plane (Bickley) jet, which has a $\text{sech}^2 y$ velocity profile, has been used by numerous authors to provide a good approximation to such a wake behind a bluff body. The Bickley jet is somewhat special in that the varicose and sinuous modes have neutral wave numbers of 1 and 2, so that the former is the subharmonic of the latter. Several studies have explored the possibility of an interaction between these two modes, and this sort of interaction is the focus of study in our papers [22] and [23]. The reason interactions between the sinuous and varicose modes are considered important is that they may give rise to extremely rapid nonlinear growth. Indeed, experimental studies have demonstrated very rapid amplification of three-dimensional disturbances in plane wakes (see, for example [24].)

In [22], we study the case of a three-dimensional disturbance with two pairs of oblique waves superimposed on the Bickley jet at the same angle, $\pm\theta$: one pair varicose, and the other sinuous. Based on the Euler equations for inviscid flows, a nonlinear critical layer analysis yields a set of highly nonlinear coupled Hickernell-type integro-differential equations for the time-evolution of the amplitudes of the disturbances. The evolution equations are solved numerically, and it is found that, as with similar problems, the evolution of the disturbance goes through three stages: initially, the disturbances grow linearly, until a second finite-amplitude nonlinear stage is reached, and eventually, the oblique waves experience explosive growth. Indeed, the numerical solutions exhibit a finite-time singularity. The origins of the singularity are not entirely clear, but it appears to be connected to the breakdown of theory, and the onset of a new, still more nonlinear stage governed by the full Euler equations. In [23], direct numerical simulation (DNS) using a standard spectral method for the viscous equations at high Reynolds number provides confirmation of our results in [22].

5 Blood Flow in Compressed Vessels

The compression of blood vessels by surrounding tissue is an important problem in hemodynamics, most prominently in studies relating to the heart. Problems related to blood flow in the cardiovascular system are accompanied by a large array of difficulties which must be overcome to completely describe the behavior of the fluid. On the other hand, many of these difficulties are not commonly encountered in engineering applications. Among these factors are the pulsation of the flow, elastic walls, non-Newtonian fluids, vessel tapering, wave reflections, and non-circular cross-sections. All of these factors interact in the determination of flow characteristics in the blood vessel system. In order to obtain quantitative results, however, it is necessary to adopt an idealization of the flow. This may involve neglecting the effects of elasticity in the wall or assuming a high degree of symmetry of the tube. To model the flow in a compressed vessel, in [25] we have approximated the membrane as a rigid elliptic cylinder. Analytical expressions for the velocity field, flow rate and wall shear stress are derived for the pulsating viscous flow. The shear stress imparted by the fluid on the walls of the membrane is known to play a role in the growth of the membrane walls. In our studies, we have shown that in a compressed regime (i.e. for large eccentricity of the elliptical walls), the shear stress may exhibit some peculiar features. In particular, well-defined peaks in the shear stress on the tube wall migrate away from their position on the minor axis of the ellipse, where they are located in steady flow.

References

[1] H.C. Pocklington. Electrical oscillations in wires. *Proc. Cambridge Phil. Soc* 9: 324-332, 1897.

[2] O.P. Bruno and M.C. Haslam. Regularity theory and super-algebraic solvers for wire antenna problems. *SIAM Journal of Scientific Computing*, **29**(4): 1375-1402, 2007.

[3] P.J. Davies, D.B. Duncan, and S.A. Funken. Accurate and efficient algorithms for frequency domain scattering from a thin wire. *J. Comput. Phys.* 168: 155-183, 2001.

[4] O.P. Bruno, M.C. Haslam, R. Paffenroth, and V.P. Cable. Mars technology program communications and tracking technologies for Mars exploration. *Proceedings of the IEEE 2006 Aerospace Conference*. D. Antsos Ed., 2006.

[5] O.P. Bruno and M.C. Haslam. Arbitrarily high-order treatment of center-fed driven wire antennas. In progress.

[6] T. T. Wu. *Introduction to linear antennas.* Inter-University Electronics Series. McGraw-Hill, New York, 1969. In: Antenna Theory Part I. Ed. R.E. Collin and F.J. Zucker.

[7] N. J. Champagne, D. R. Wilton, and J. D. Rockway. The analysis of thin wires using higher order elements and basis functions. *IEEE Trans. Antennas Propagat.*, 54(12):3815–3821, 2006.

[8] O.P. Bruno and M.C. Haslam. Fast high-order methods for large driven wire arrays. In progress.

[9] O.P. Bruno and M.C. Haslam. Super-algebraic solvers for three-dimensional curved wire antennas. In progress.

[10] O.P. Bruno and M.C. Haslam. Efficient high-order evaluation of scattering by periodic surfaces: deep gratings, high frequencies and glancing incidences. *Journal of the Optical Society of America A*, **26**(3): 658–668, 2009.

[11] O.P. Bruno and M.C. Haslam. Efficient high-order evaluation of scattering by periodic surfaces: vector-parametric gratings and geometric singularities. *Waves in Random and Complex Media*, Accepted, 2010.

[12] M.C. Haslam. A study of anomalous scattering from lamellar diffraction gratings. *Canadian Applied Math Quarterly*, Accepted, 2010.

[13] D. Colton and R. Kress. *Inverse acoustic and electromagnetic scattering theory*, volume 93 of *Applied Mathematical Sciences*. Springer-Verlag, Berlin, second edition, 1998.

[14] M.C. Haslam. Efficient solution of the scattering problem for layered dielectric gratings. In progress

[15] J. DeSanto, G. Erdmann, W. Hereman, and M. Misra. Theoretical and computational aspects of scattering from rough surfaces: one-dimensional perfectly reflecting surfaces. *Waves Random Media*, 8(4):385–414, 1998.

[16] O.P. Bruno and L. Kunyansky. A fast, high-order algorithm for the solution of surface scattering problems: basic implementation, tests and applications. *J. Comput. Phys.* 169: 80-110, 2001.

[17] M.C. Haslam. Electromagnetic Scattering from Doubly Periodic Dielectric Surfaces With Application to Ocean Physics and Remote Sensing (Ph.D. thesis). Submitted to the Faculty of Graduate Studies, University of Western Ontario, December. 2002.

[18] M.C. Haslam and R. Mallier. Vortices on a cylinder *Physics of Fluids* **15**(7): 2087-2088, 2003.

[19] R.W.P. King. *The Theory of Linear Antennas With Charts and Tables for Practical Applications.* Harvard University Press. Cambridge, MA, 1956.

[20] B.L. Lewis and I.D. Olin. Experimental study and theoretical model of high-resolution radar backscatter from the sea. *Radio Science* 15: 815-828, 1980.

[21] J.W. McLean. Instabilities of finite-amplitude water waves *J. Fluid Mech.* 114 : 315-330, 1982.

[22] R. Mallier and M. Haslam. Interactions between pairs of oblique waves in a Bickley jet. *Eur. J. Mech. B/Fluids* 18(2): 227-243, 1999.

[23] R. Mallier and M. Haslam. Modal interactions in a Bickley jet: comparison of theory with direct numerical simulation. *Mathematics and Computers in Simulation* 62: 109-115, 2003

[24] T.C. Corke, M. Krull and J.D. Ghassemi. Three-dimensional resonance in far wakes *J. Fluid Mech.* 239 : 99-132, 1992.

[25] M.C. Haslam and M. Zamir. Pulsatile flow in tubes of elliptic cross sections. *Annals Biomedical Engineering* 26(5): 780-787, 1998.